

Optimizing Perturbations for Improved Training of Machine Learning Models

Sagi Meir,^{1,2} Tommer D. Keidar,^{1,2} Shlomi Reuveni,^{1,2,3} and Barak Hirshberg^{1,2,3,*}

¹*School of Chemistry, Tel Aviv University, Tel Aviv 6997801, Israel.*

²*The Center for Physics and Chemistry of Living Systems, Tel Aviv University, Tel Aviv 6997801, Israel.*

³*The Center for Computational Molecular and Materials Science, Tel Aviv University, Tel Aviv 6997801, Israel.*

Machine learning models have become indispensable tools in applications across the physical sciences. Their training is often time-consuming, vastly exceeding the inference timescales. Several protocols have been developed to perturb the learning process and improve the training, such as shrink and perturb, warm restarts, and stochastic resetting. For classifiers, these perturbations have been shown to result in enhanced speedups or improved generalization. However, the design of such perturbations is usually done *ad hoc* by intuition and trial and error. To rationally optimize training protocols, we frame them as first-passage processes and consider their response to perturbations. We show that if the unperturbed learning process reaches a quasi-steady state, the response at a single perturbation frequency can be used to predict the behavior at a wide range of frequencies. We demonstrate that this is the case when training a CIFAR-10 classifier using the ResNet-18 model, and use this approach to identify an optimal perturbation and frequency. Our work allows optimization of training protocols of machine learning models using a statistical mechanical approach.

Keywords: machine learning, neural networks, statistical physics, perturbations, stochastic resetting, first-passage, response theory

I. INTRODUCTION

Machine learning algorithms and deep neural network (NN) models have become powerful tools across chemistry and physics to tackle challenges that were once computationally or experimentally prohibitive. Examples include protein structure prediction [1], entropy calculation for physical systems [2], machine learning potentials [3], and many others [4–11]. Unfortunately, these capabilities come with a time-consuming price spent on model training. Second-order optimization algorithms are unfeasible for deep NN [12, 13], and currently, stochastic gradient descent (SGD) and its variants, remain a cornerstone of NN training [13–20].

SGD by itself can be slow and prone to getting stuck in local minima. Several common practices are used to address these limitations. First is the incorporation of momentum and adaptive learning rates as done by modern optimizers, usually leading to faster convergence and improved performance [18–21]. The second, which is the focus of this work, is to “perturb” the training process, which may lead to speedup or improved generalization. Examples include shrink & perturb (S&P) [22, 23], warm restarts [13], stochastic resetting (SR) [24] and continual backpropagation [25].

Ash et al. [22] first suggested the S&P protocol to improve generalization during online learning. More recently, Zaidi et al. [23] investigated when such re-initialization might help the training, and concluded that while it is clear S&P is helpful in some cases, a general theory of why it works is missing. Bae et al. [24] applied SR during the training of an NN, to a dynamically-updated checkpoint with a resetting time sampled from an exponential distribution. They concluded that their strategy decreases overfitting on noisy labels and leads to better generalization. Yet, predicting the optimal resetting rate a priori was not possible. Loshchilov et al. [13] showed that a protocol with warm restarts converges up to four times faster to the same test accuracy compared to standard SGD training. Overall, despite their usefulness, a theory capable of predicting the effect of such perturbation protocols is missing, and their design is often done by intuition and empirical trial and error.

The resemblance of SGD to Langevin dynamics [26, 27] has been utilized to describe and analyze the learning process of NNs with concepts and methods from thermodynamics and statistical physics [26, 28–35]. For example, Feng et al. found an inverse fluctuation-dissipation relation between weights’ fluctuations and the flatness of the loss landscape. Based on their finding they developed an algorithm that delays catastrophic forgetting in sequential learning tasks [26].

* hirshb@tauex.tau.ac.il

Another example is the work of Stephan et al. where they showed that SGD with a constant learning rate can be used as an approximate Bayesian posterior inference algorithm [31]. Their result was obtained by viewing SGD as a Markov chain with a stationary distribution. However, despite the advancements in applying statistical mechanical tools in machine learning, they have not been previously used to design perturbations to improve the performance of SGD optimizers.

Recently, Keidar et al. developed a response theory to predict how rare perturbations affect the completion of an arbitrary stochastic process [36]. Their theory focused on first-passage processes [37–44], in which a stochastic process has a predefined distribution of initial conditions and a well-defined endpoint. The stochastic nature of the process gives rise to a distribution of first-passage times, i.e., the first time the process reaches one of its endpoints. In this work, we treat the SGD-based training of NNs up to a predefined accuracy as a first-passage process. We treat protocols such as S&P, warm restarts, and stochastic resetting as perturbations to the first-passage process that occur every P epochs during the training. We employ the theory of Keidar et al. for the first time to analyze and improve the training of NN models using such perturbations. We show that, given a set of protocols, we can determine which would lead to the highest acceleration and identify the optimal perturbation time interval P . We focus on three types of protocols: S&P, partial re-initialization of small weights, and full SR. Finally, we suggest a new methodology for testing and analyzing new training protocols that reduce the number of experiments.

II. THEORY

In this work, we treat the NN training in the absence of a perturbation as a stochastic process that is characterized by a propagator $G(\boldsymbol{\theta}, t)$, representing the probability of being in state $\boldsymbol{\theta}$ at time t . We emphasize that $\boldsymbol{\theta}$ characterizes the overall state of the system, i.e., it may represent the weights, biases, hyperparameters, etc. We focus on first-passage processes (see Fig. 1A), and define the first-passage time (FPT) as the first instance in which the test accuracy reaches a certain threshold, which is treated as an absorbing boundary condition. Namely, the propagator includes only trajectories that have not reached this point. Since it is a stochastic process, there will be an FPT distribution. We denote with T the random variable representing the FPT of the unperturbed training process. We define the survival probability $\Psi_T(t)$, i.e., the fraction of models which did not reach the threshold at time t , as

$$\Psi_T(t) = \int_{\Theta} G(\boldsymbol{\theta}, t) d\boldsymbol{\theta}, \quad (1)$$

where Θ represents integration over all possible states.

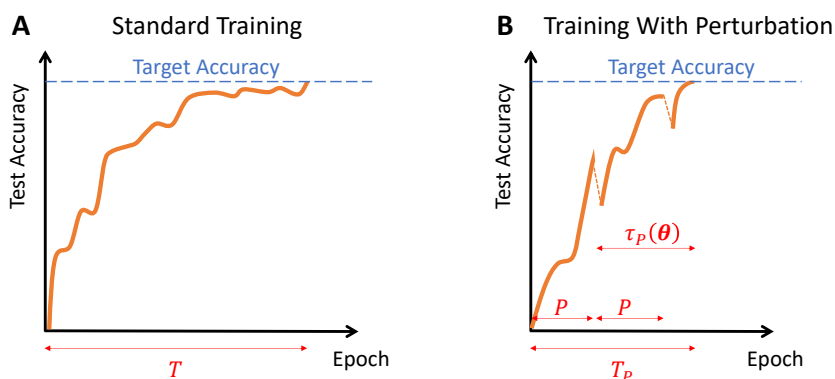


Figure 1. Training NNs as a first-passage process. Panel A presents the test accuracy as a function of the number of epochs for training without perturbations (orange line). Here, T is the FPT to reach the target accuracy (dashed blue line). Panel B presents the test accuracy as a function of the number of epochs for training with a perturbation every P epochs (orange line). T_P is the perturbed FPT to the target accuracy (dashed blue line) and $\tau_P(\boldsymbol{\theta})$ is the residual time to reach the target accuracy after the first perturbation.

Fig. 1B shows the training process with the perturbation, which is applied every P epochs. We denote by T_P the random variable representing the FPT of the perturbed process to the target accuracy. The perturbation can be of any form, e.g., it can affect the network weights, hyperparameters, activation functions, or any other component of the training. Keidar et al. showed that the perturbed FPT is connected to the unperturbed FPT through, [36]

$$T_P = \begin{cases} T & \text{if } T \leq P, \\ P + \tau_P(\boldsymbol{\theta}) & \text{if } T > P, \end{cases} \quad (2)$$

where $\tau_P(\boldsymbol{\theta})$ is the random variable representing the residual number of epochs it takes to reach the first-passage criterion after the perturbation has been first applied (see Fig. 1B). It depends on $\boldsymbol{\theta}$, the state of the network at time P , which might be different for every realization of the process.

Applying the law of total expectation to Eq. (2) (see the derivation in the appendix), we obtain the mean FPT under perturbations, $\mathbb{E}[T_P]$,

$$\mathbb{E}[T_P] = \sum_{t=0}^{P-1} \Psi_T(t) + \Psi_T(P) \bar{\tau}_P, \quad (3)$$

where $\bar{\tau}_P$ is given by

$$\bar{\tau}_P = \int_{\Theta} \mathbb{E}[\tau_P(\boldsymbol{\theta})] \frac{G(\boldsymbol{\theta}, P)}{\Psi_T(P)} d\boldsymbol{\theta}. \quad (4)$$

In Eq. (4), $\mathbb{E}[\tau_P(\boldsymbol{\theta})]$ is the average residual time after the first perturbation over all possible noise realizations of the stochastic training process after the perturbation was applied to a given state $\boldsymbol{\theta}$ at time P . Hence, $\bar{\tau}_P$ can be understood as the average of $\mathbb{E}[\tau_P(\boldsymbol{\theta})]$ over all possible $\boldsymbol{\theta}$ generated by the unperturbed process at time P right before the perturbation has been applied.

Eq. (3) formally decomposes the mean FPT with the perturbation to two contributions. The first term, $\sum_{t=0}^{P-1} \Psi_T(t)$, sets a lower bound on $\mathbb{E}[T_P]$ that only depends on the underlying unperturbed process. The second term encodes all the effects of the perturbation on the mean FPT. These equations allow, in principle to predict the effect of a perturbation on the training for all P .

Consider, for example, the specific case of SR as the perturbation. Then, every P epochs, the state of the system is restarted by resampling the initial conditions for training. As a result, for any training process, $\tau_P(\boldsymbol{\theta})$ does not depend on the state at time P , and is simply an independent and identically distributed copy of T_P . In that case, $\bar{\tau}_P = \mathbb{E}[T_P]$, and substituting it into Eq. (3) gives, [45]

$$\mathbb{E}[T_P]_{SR} = \frac{1}{1 - \Psi_T(P)} \sum_{t=0}^{P-1} \Psi_T(t). \quad (5)$$

Eq. (5) shows that, for SR, the mean FPT with the perturbation can be predicted entirely from the survival probability of the unperturbed learning process.

To derive, Eq. (5), we used the specific properties of SR. For other perturbations, one must assume something about the dynamics of the underlying training process.

III. RESULTS AND DISCUSSION

A. The quasi-steady state hypothesis

To proceed beyond Eq. (3), we consider a stochastic process in which the propagator reaches a quasi-steady state (QSS) after a typical relaxation time t_r ,

$$G(\boldsymbol{\theta}, t) \simeq \phi(\boldsymbol{\theta}) \Psi_T(t) \quad \text{for } t > t_r. \quad (6)$$

In Eq. (6), $\phi(\boldsymbol{\theta})$ is a time-independent probability density function of the network state $\boldsymbol{\theta}$. In other words, a QSS is defined by constant relative populations of all states $\boldsymbol{\theta}$, although the overall number of models that survived

declines over time through $\Psi_T(t)$ [46], as illustrated in Fig. 2. The QSS approximation is commonly applied to analyze chemical kinetics [46–50], but has not been used to explain NN training before. Next, we use it to show that for rare perturbations, the mean residual time $\bar{\tau}_P$ is independent of P . Therefore, by using samples of the training at a single value of P , i.e., a single perturbation frequency, we can predict the mean FPT at a wide range of perturbation frequencies.

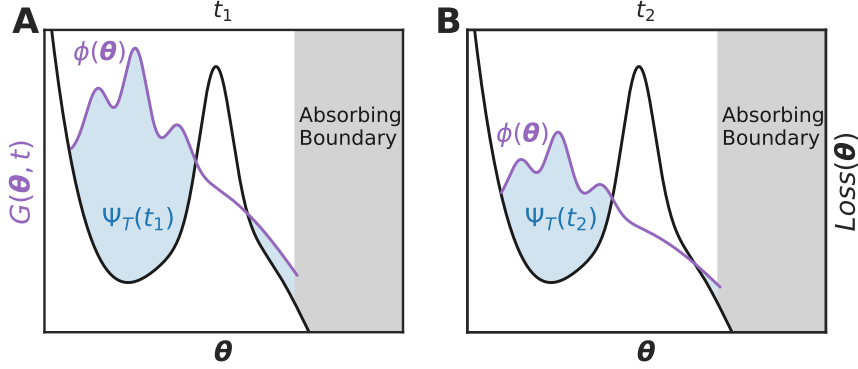


Figure 2. An illustration of a QSS of a propagator $G(\boldsymbol{\theta}, t)$ at times $t_2 > t_1 > t_r$. At QSS, the probability density function $\phi(\boldsymbol{\theta})$ (purple lines) maintains the same shape, while the fraction of models that survived (blue areas) declines over time through panels A-B, i.e., $\Psi_T(t_1) > \Psi_T(t_2)$.

To show this, we consider three timescales in the system: the relaxation time t_r , the perturbation time interval P and the mean residual time for completion after applying the perturbation $\bar{\tau}_P$. Considering a perturbation that is done at a time $P > t_r$, and utilizing QSS, we observe that the perturbation acts on a state sampled from $\phi(\boldsymbol{\theta})$ irrespective of P . We can then plug Eq. (6) into Eq. (4) and get

$$\bar{\tau}_P = \int_{\Theta} \mathbb{E}[\tau_P(\boldsymbol{\theta})] \phi(\boldsymbol{\theta}) d\boldsymbol{\theta}. \quad (7)$$

Note that the mean residual time for completion after the perturbation is applied still depends on P through $\mathbb{E}[\tau_P(\boldsymbol{\theta})]$. Next, if the perturbation is rare enough, i.e., $P > \bar{\tau}_P$, we effectively perturb the system only once on average before the training is complete. As a result, $\tau_P(\boldsymbol{\theta}) = \tau(\boldsymbol{\theta})$, i.e., does not depend on P , leading to

$$\bar{\tau}_P \approx \bar{\tau} = \int_{\Theta} \mathbb{E}[\tau(\boldsymbol{\theta})] \phi(\boldsymbol{\theta}) d\boldsymbol{\theta} \quad \text{for } P > \max(t_r, \bar{\tau}_P). \quad (8)$$

Plugging Eq. (8) into Eq. (3) leads to

$$\mathbb{E}[T_P] = \sum_{t=0}^{P-1} \Psi_T(t) + \Psi_T(P) \bar{\tau}. \quad (9)$$

Eq. (9) sets the recipe for designing useful perturbations and the frequencies at which to apply them. It tells us to perform simulations applying the perturbation only once at some $P^* > \max(t_r, \bar{\tau}_P)$. These simulations provide the unbiased survival function until time P^* and $\bar{\tau}$. Combining the two, we can predict the mean FPT for all values $\max(t_r, \bar{\tau}_P) \leq P \leq P^*$.

Below, we first show that a QSS is reached when training a CIFAR-10 [51] classifier using the ResNet-18 model [52]. Then, for two perturbations, S&P and partial resetting, we show that indeed $\bar{\tau}_P \approx \bar{\tau}$ for a wide range of P . Finally, we use Eq. (9) to predict the behavior of these perturbations at all P , benchmark them against brute-force training, and show that this procedure can be used to select the perturbation type and time P that lead to a higher generalization or faster training.

B. Experimental test of the quasi-steady-state

A naive approach to demonstrate a QSS when training an NN model would be to sample several learning trajectories while keeping track of the parameters to obtain $G(\boldsymbol{\theta}, t)$. However, it is impractical to keep track of millions of parameters, and the finite sample size introduces noise to the estimation of the distribution of $G(\boldsymbol{\theta}, t)$. This noise increases with the dimensionality of $\boldsymbol{\theta}$, making it infeasible to demonstrate a QSS convergence from the trajectory data of $\boldsymbol{\theta}$. Instead, we draw inspiration from enhanced sampling of free energy surfaces [53–55] and define a collective variable, $A(\boldsymbol{\theta})$, representing the state of the system and look at its marginal distribution,

$$G(A, t) = \int_{\Theta} G(\boldsymbol{\theta}, t) \delta(A(\boldsymbol{\theta}) - A) d\boldsymbol{\theta}. \quad (10)$$

In practice, we will use the test set accuracy as a collective variable. If $G(\boldsymbol{\theta}, t)$ reaches a QSS, and we plug Eq. (6) into Eq. (10), we get a QSS also in $G(A, t)$,

$$G(A, t) \simeq \Psi_T(t) \int_{\Theta} \phi(\boldsymbol{\theta}) \delta(A(\boldsymbol{\theta}) - A) d\boldsymbol{\theta} = \Psi_T(t) \phi(A), \quad \text{for } t > t_r. \quad (11)$$

In Eq. (11), $\phi(A) = \int_{\Theta} \phi(\boldsymbol{\theta}) \delta(A(\boldsymbol{\theta}) - A) d\boldsymbol{\theta}$ is the time-independent probability density function of A . Therefore, we will use the dynamics of $G(A, t)$ as a proxy to justify the QSS hypothesis.

We used the ResNet-18 architecture as our NN model for the classification task of the CIFAR-10 dataset. We trained 1000 models using random initialization and plotted the test accuracy as a function of the number of epochs, which we will refer to as trajectories. We used standard SGD training, without perturbations. See the Computational Details section for the full training setup. To obtain the propagator $G(A, t)$ from the trajectory data for a specific test accuracy target, we treat it as an absorbing boundary. In other words, trajectories that reached the target accuracy are stopped and excluded from $G(A, t)$ at later times. $\Psi_T(t)$ is estimated by the fraction of models that did not reach the target at epoch t of the training (see Eq. (1)).

In Fig. 3A, we start by analyzing the specific case of a target test accuracy of 75% (dashed blue line). For this accuracy, no model reaches the target up to 100 epochs, i.e., $\Psi_T(t) = 1 \forall t$ (blue line Fig. 3C). The violins of Fig. 3A represent the density distribution of A as a function of time. It narrows down with time, until epoch ~ 20 , and then remains with a fixed shape and height, which suggests that $G(A, t) = \phi(A)$ from that epoch onwards. Besides this qualitative shape comparison, we also quantitatively compare the cumulative distribution functions (CDFs) of A to the average CDF of A over epochs 20 to 100 with the Kolmogorov–Smirnov (KS) test [56–58], shown in Fig. 3D (blue line). We define the relaxation time as having a p-value larger than 0.05 in the KS test, which gives a relaxation time of $t_r = 17$ epochs. Alternative statistical tests result in similar relaxation times (see the appendix).

In Fig. 3B we set the target test accuracy to 72% which leads to a decay of $\Psi_T(t)$ with the number of epochs, i.e., some trajectories reach the target during the training (orange line in Fig. 3C). Although there is a decline in the number of models that did not reach the target, after ~ 30 epochs the shape of the density distribution again remains approximately fixed while the height decreases, as expected from a QSS (Eq. (11)). We compare the CDFs of A to the average CDF of A over epochs 20 to 100 with the KS test [56–58], conditioned on model survival. Similarly to the previous case, we plot the p-value of the KS-test in Fig. 3D (orange line) and obtain $t_r = 28$ epochs. We also checked the QSS hypothesis for a lower target accuracy of 71.5% and plot the survival function and KS-test p-value in Fig. 3C,D (green lines), respectively. Again, we obtain a similar relaxation time of $t_r = 26$ epochs. All these examples confirm our hypothesis, demonstrating that the training of a CIFAR-10 classifier using a ResNet-18 model reaches a QSS for various target accuracies.

C. Experimental test that the residual time is P -independent

We have shown in the previous section that our NN model reaches a QSS. Next, we show that if P is large enough, introducing a perturbation would result in P -independent residual times, according to Eq. (8). Here, we show it experimentally by focusing on the 72% test accuracy target case (Fig. 3B) where the system reaches a QSS after $t_r = 28$ epochs. We analyze the dependence of the residual time to reach the target on the perturbation time P . To do so, we take only the models that did not reach the target after $P = 100, 50, 20,$ and 10 epochs, introduce the perturbation, and continue the training until reaching the target. consider two perturbations, S&P and partial SR.

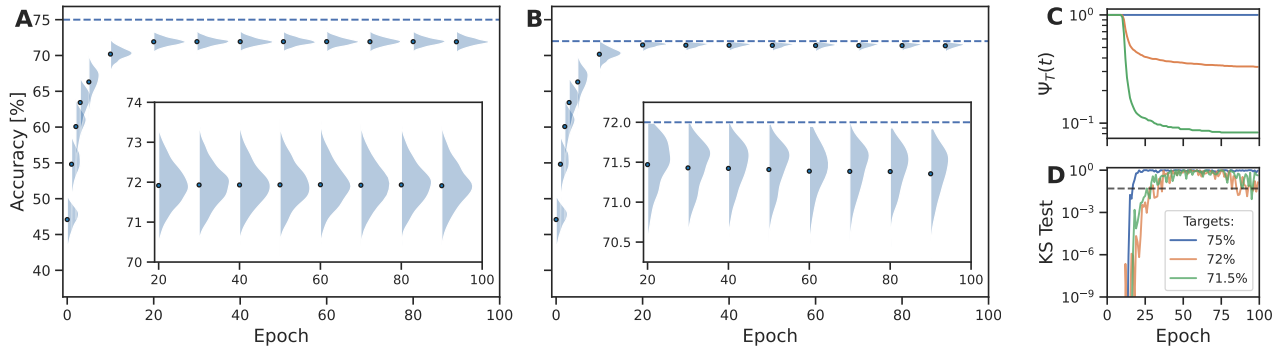


Figure 3. Experimental evidence for a quasi-steady-state. Panels A and B are violin plots of the density distributions of the test accuracy as a function of the number of epoch, for models that did not reach the target. Blue dots represent the mean accuracy and the blue areas are the distributions rotated by 90°. The dashed blue lines are the target accuracies, set to 75% and 72% in panels A and B, respectively. In both cases, after ~ 20 -30 epochs, the system reaches a quasi-steady state, i.e., $G(A, t) \simeq \phi(A)\Psi_T(t)$. Panel A is a special case in which $\Psi_T(t) = 1$, while in panel B, $\Psi_T(t)$ decays slowly. Panel C shows the survivals $\Psi_T(t)$ for the 75% (blue), 72% (orange), and 71.5% (green) target test accuracies. Panel D is the Kolmogorov–Smirnov (KS) test between the CDFs of the accuracy A at different epochs to the average CDF of A over epochs 20 to 100.

The S&P perturbation takes the weights and biases of the NN at the moment it is applied, shrinks them by a factor λ and adds an independent and identically distributed copy sampled from the initial conditions distribution, multiplied by a factor γ . We used the same values used by [23], $\lambda = 0.4$ and $\gamma = 0.1$. The partial SR perturbation takes only a fraction of the parameters of the NN and re-initializes them to an independent and identically distributed copy sampled from the initial conditions distribution. We chose to initialize 30% of the weights, those with the smallest absolute value at the moment the perturbation is applied.

In Fig. 4, we first plot the mean test accuracy of the models as a function of the epoch. The top and bottom rows correspond to the S&P and the partial resetting perturbations, respectively. In all cases, we find that the residual time of the mean trajectory to reach the target is smaller than P and that the perturbation is only applied once before reaching the target. As a result, when $P > t_r$, we expect that the mean residual time will be P -independent, as explained in Section III A. In panels E and J we center all the mean trajectories with respect to their perturbation time P . We find that all curves approximately collapse on top of each other regardless of P , reaching the target accuracy after the same number of epochs since the perturbation has been applied (gray area). We emphasize that the residual time is different for the two perturbations, as shown in panels E and J, but is P -independent in both cases.

Next, instead of plotting the average training curve, we plot the value of the residual time $\bar{\tau}_P$ as a function of P in Fig. 5 for a larger range of $P = 1$ –100. We observe that $\bar{\tau}_P$ is roughly constant over nearly two orders of magnitude in P for both perturbations, showing that the QSS hypothesis holds for a wide range of perturbation times. Surprisingly, $\bar{\tau}_P \approx \bar{\tau}$ even for values of P that are smaller than the relaxation time. However, when P becomes smaller than the residual time (~ 3 and ~ 5 for S&P and partial SR, respectively), denoted by the shaded area in Fig. 5, the process is perturbed more than once on average before reaching the target and the residual time is no longer P -independent.

D. Prediction of the mean FPT

In this section, we show how to predict the mean FPT with a perturbation for a wide range of P from as few samples as possible. We begin by assuming that several training trajectories are already available, and we wish to assess whether applying a perturbation is worthwhile, and select at what time interval to apply it. The simplest perturbation to analyze is SR. It comes at no additional cost, through Eq. (5), since we already sampled the survival function. To quantify the acceleration in reaching a target accuracy by applying a perturbation, we define the speedup as the ratio between the mean FPT without and with the perturbation, respectively. We plot the predicted speedup for SR in Fig. 6 (blue line) and compare it with numerical experiments (blue squares). We find

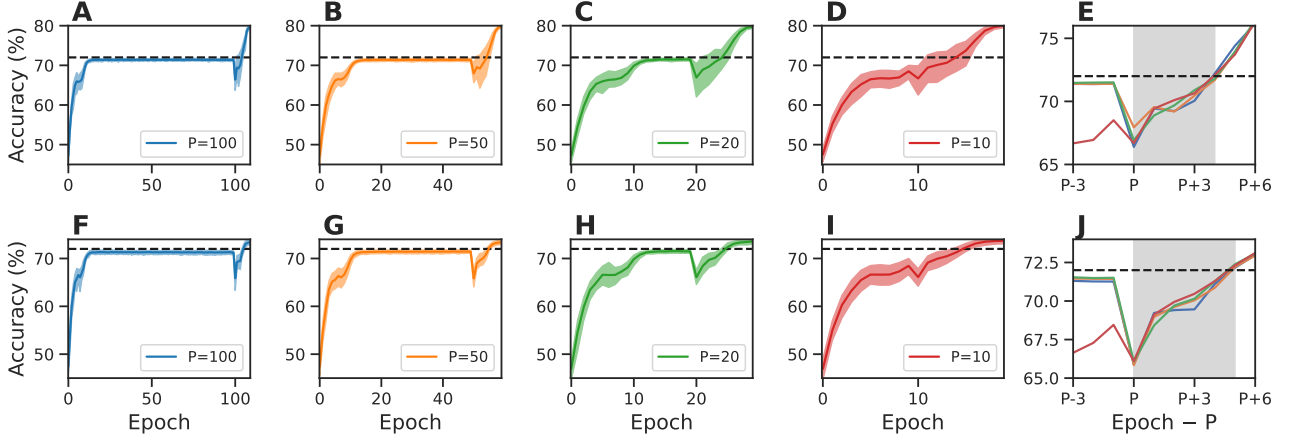


Figure 4. The mean trajectories of the test accuracy and their top and bottom deciles (shaded areas), that did not reach 72% test accuracy after P epochs. From left to right $P = 100, 50, 20, 10$ (see legend). The dashed black lines represent 72% test accuracy (the target). At epoch number P we apply the S&P protocol (upper row, panels A-E) or the partial resetting protocol (lower row, panels F-J). Panels E and J center the mean trajectories with respect to their P . The gray areas are from the moment of perturbation until a the first time that the average trajectory reaches the target accuracy.

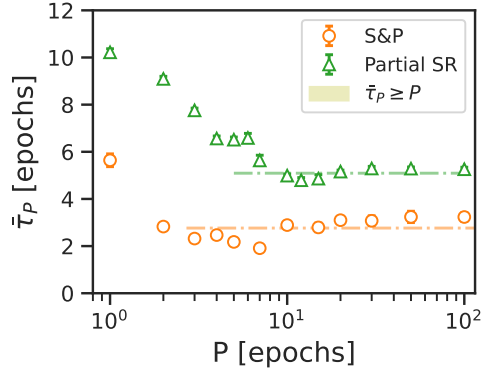


Figure 5. $\bar{\tau}_P$ versus the perturbation time. The values of $\bar{\tau}_P$ for S&P (orange circles) and partial SR (green triangles) are approximately constant when $P > \bar{\tau}_P$ (outside the yellow area). Dashed dotted lines are averages of all $\bar{\tau}_P < P$.

that SR leads to a maximal speedup of ~ 3 using a perturbation time interval of ~ 20 .

To go beyond SR to other perturbations that could potentially lead to higher speedups, we must measure their residual time. A naive approach of simply evaluating $\bar{\tau}_P$ for every P and using Eq. (3) would mean running the training for all perturbations at all P values, which is costly. Instead, we would like to use the fact that the residual time is P -independent. To that end, we sample the training with the perturbation applied once at some P^* that is large enough. We then use Eq. (9) to predict the mean FPT for a wide range of $P < P^*$. We plot the predicted speedup in Fig. 6 for the S&P (orange line) and partial SR (green line) perturbations, using their value of $\bar{\tau}_{P^*}$ at $P^* = 100$. Going from right to left on the P axis, the predictions fit the experimental values of the S&P (orange circles) and partial SR (green triangles) protocols for $P \geq \bar{\tau}_{P^*}$, as expected.

Using these predictions, we identify that S&P leads to a speedup of ~ 16 at a perturbation time interval of 3, while partial SR leads to a speedup of ~ 8 at $P = 7$. These predictions correctly identify S&P as the preferred

strategy that leads to the highest speedup. Although the experimental maximal speedup is slightly larger (~ 21), our predictions are a computationally efficient way of determining useful perturbations and time intervals that lead to high speedups.

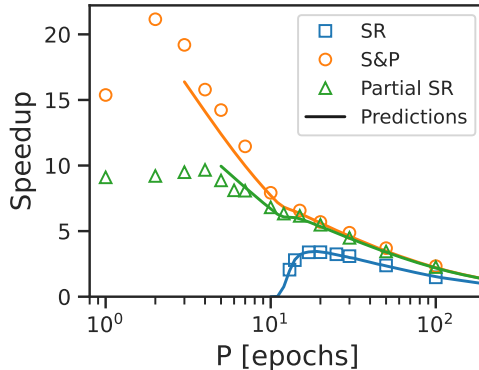


Figure 6. The speedup gained by using different perturbation protocols versus the perturbation time. Orange and green solid lines are the theoretical predictions of Eq. (9) for S&P and partial SR, respectively. For the predictions, we used the value of $\bar{\tau}_{P^*}$ for $P^* = 100$. We plot the predictions only down to $P = \bar{\tau}_{P^*}$. The blue solid line is the theoretical prediction for the SR case (Eq. (5)). Symbols represent brute force training at every value of P .

We suggest a general methodology that can examine different kinds of perturbations and pick the optimal one and an efficient P . We rely on common practices that are used to train NNs. Consider for example a classification task for which the architecture of the NN and the hyperparameters of the SGD-based optimization are predetermined. Then, it is common practice to train in parallel an ensemble of models and terminate any training process that did not reach a minimal desired test accuracy after a tolerance time of P^* epochs. After this process is completed, we propose to estimate the survival function, $\Psi_T(t)$ for $t \leq P^*$. This is already enough information to evaluate whether SR leads to any acceleration. For other perturbations, evaluate first if the unperturbed process has reached a QSS and determine $t_r < P^*$. If that is the case, introduce several candidate perturbations to the models that did not reach the target accuracy and measure $\bar{\tau}_{P^*}$ for each one. This way, $\Psi_T(t \leq P^*)$ and $\bar{\tau}_{P^*}$ are obtained simultaneously for several perturbation protocols. According to Eq. (9), the perturbation with the minimal $\bar{\tau}_{P^*}$ is the preferred one. Finally, to obtain an efficient perturbation time interval, plug $\Psi_T(t \leq P^*)$ and $\bar{\tau}_{P^*}$ into Eq. (9), and evaluate the speedup for $\max(t_r, \bar{\tau}_{P^*}) \leq P \leq P^*$. Choose the time interval that leads to the highest speedup.

IV. SUMMARY AND CONCLUSION

We developed an approach based on a recent response theory by Keidar et al. [36] to design useful perturbations for accelerating the training of NNs. To that end, we treated the training as a first-passage process to a target test accuracy. For the case of a CIFAR-10 classifier using the ResNet-18 architecture, we demonstrated that the unperturbed training process reached a QSS after a relaxation time of 20-30 epochs. We showed that, as a result, we can predict the mean FPT for a wide range of perturbation times from measurements at a single perturbation time. Lastly, we proposed a strategy to examine different kinds of perturbations and pick the optimal one and an efficient P . We showed that this strategy correctly selects S&P as a better perturbation than partial SR or SR for a CIFAR-10 classifier and identified a useful perturbation time. Our work provides a statistical mechanical framework capable of identifying perturbations that result in a speedup when training an NN model up to a target accuracy. It allows for a more rational design of training protocols, based on physical insights.

V. COMPUTATIONAL DETAILS

The CIFAR-10 dataset contains 50,000 training and 10,000 test RGB images each belonging to one of 10 different classes. The number of images per class across the train and test sets is equal, and each image is 32×32 pixels in size. For classification, we used a common modified version of the ResNet-18 architecture, because the original architecture was designed for much larger images. The modification includes reducing the kernel size of the first convolution layer from 7 to 3, the stride from 2 to 1, and the padding from 3 to 1. We also removed the subsequent max pooling layer to maintain everything else similar to the original architecture (as was done in the work of Zaidi et al. [23]).

We did not use any data augmentation techniques except for standard data normalization (by the channel-wise mean and variance of the train images) for both train and test datasets. We initialized the weights and biases with the default initialization of Pytorch, i.e., uniform distribution, and used the FFCV library for faster training [59]. We trained each model with an SGD optimizer with a learning rate of 0.02. Implementation of the perturbations was straightforward according to their definitions above. The test accuracy curves for each perturbative protocol with $P = 20$ are presented in supporting information.

ACKNOWLEDGEMENTS

B.H. acknowledges support from the Israel Science Foundation (grants No. 1037/22 and 1312/22) and the Pazy Foundation of the IAEC-UPBC (grant No. 415-2023). This project has received funding from the European Research Council (ERC) under the European Union’s Horizon 2020 research and innovation program (grant agreement No. 947731 to S.R.). S.M. acknowledges support from the Quantum Science and Technology Center of Tel Aviv University. B.H. and S.M. thank Sheheryar Zaidi for sharing his code. The authors thank Yohai Bar Sinai, Tomer Koren, and Rotem Widman for fruitful discussions.

-
- [1] J. Jumper, R. Evans, A. Pritzel, T. Green, M. Figurnov, O. Ronneberger, K. Tunyasuvunakool, R. Bates, A. Židek, A. Potapenko, *et al.*, *Nature* **596**, 583 (2021).
 - [2] A. Nir, E. Sela, R. Beck, and Y. Bar-Sinai, *Proceedings of the National Academy of Sciences* **117**, 30234 (2020).
 - [3] J. Behler and M. Parrinello, *Physical review letters* **98**, 146401 (2007).
 - [4] G. Carleo and M. Troyer, *Science* **355**, 602 (2017).
 - [5] F. Noé, S. Olsson, J. Köhler, and H. Wu, *Science* **365**, eaaw1147 (2019).
 - [6] B. Máté, F. Fleuret, and T. Berau, *The Journal of Physical Chemistry Letters* **15**, 11395 (2024).
 - [7] A. Anelli, H. Dietrich, P. Ectors, F. Stowasser, T. Berau, M. Neumann, and J. van den Ende, *CrystEngComm* **26**, 5845 (2024).
 - [8] C. Lagemann, K. Lagemann, S. Mukherjee, and W. Schröder, *Nature Machine Intelligence* **3**, 641 (2021).
 - [9] S. Ravuri, K. Lenc, M. Willson, D. Kangin, R. Lam, P. Mirowski, M. Fitzsimons, M. Athanassiadou, S. Kashem, S. Madge, *et al.*, *Nature* **597**, 672 (2021).
 - [10] Y. Wang, J. M. L. Ribeiro, and P. Tiwary, *Current opinion in structural biology* **61**, 139 (2020).
 - [11] S.-T. Tsai, E.-J. Kuo, and P. Tiwary, *Nature communications* **11**, 5115 (2020).
 - [12] K. Fukumizu and S.-i. Amari, *Neural networks* **13**, 317 (2000).
 - [13] I. Loshchilov and F. Hutter, *arXiv preprint arXiv:1608.03983* (2016).
 - [14] X. Peng, L. Li, and F.-Y. Wang, *IEEE transactions on neural networks and learning systems* **31**, 4649 (2019).
 - [15] G. Nguyen, S. Dlugolinsky, M. Bobák, V. Tran, Á. López García, I. Heredia, P. Malík, and L. Hluchý, *Artificial Intelligence Review* **52**, 77 (2019).
 - [16] D. E. Rumelhart, G. E. Hinton, and R. J. Williams, *nature* **323**, 533 (1986).
 - [17] J. Duchi, E. Hazan, and Y. Singer, *Journal of machine learning research* **12** (2011).
 - [18] I. Sutskever, J. Martens, G. Dahl, and G. Hinton, in *International conference on machine learning* (PMLR, 2013) pp. 1139–1147.
 - [19] M. D. Zeiler, *arXiv preprint arXiv:1212.5701* (2012).
 - [20] D. P. Kingma, *arXiv preprint arXiv:1412.6980* (2014).
 - [21] B. Leimkuhler, C. Matthews, and T. Vlaar, *Foundations of Data Science* **1**, 457 (2019).
 - [22] J. Ash and R. P. Adams, *Advances in neural information processing systems* **33**, 3884 (2020).
 - [23] S. Zaidi, T. Berariu, H. Kim, J. Bornschein, C. Clopath, Y. W. Teh, and R. Pascanu, in *Proceedings on* (PMLR, 2023) pp. 12–26.

- [24] Y. Bae, Y. Song, and H. Jeong, arXiv preprint arXiv:2406.00396 (2024).
- [25] S. Dohare, J. F. Hernandez-Garcia, Q. Lan, P. Rahman, A. R. Mahmood, and R. S. Sutton, *Nature* **632**, 768 (2024).
- [26] Y. Feng and Y. Tu, *Proceedings of the National Academy of Sciences* **118**, e2015617118 (2021).
- [27] X. Cheng, D. Yin, P. Bartlett, and M. Jordan, in *International Conference on Machine Learning* (PMLR, 2020) pp. 1810–1819.
- [28] H. S. Seung, H. Sompolinsky, and N. Tishby, *Physical review A* **45**, 6056 (1992).
- [29] A. Choromanska, M. Henaff, M. Mathieu, G. B. Arous, and Y. LeCun, in *Artificial intelligence and statistics* (PMLR, 2015) pp. 192–204.
- [30] A. A. Alemi and I. Fischer, arXiv preprint arXiv:1807.04162 (2018).
- [31] M. Stephan, M. D. Hoffman, and D. M. Blei, *Journal of Machine Learning Research* **18**, 1 (2017).
- [32] T. Jules, G. Brener, T. Kachman, N. Levi, and Y. Bar-Sinai, arXiv preprint arXiv:2304.01335 (2023).
- [33] L. Zdeborová, *Nature Physics* **16**, 602 (2020).
- [34] G. E. Karniadakis, I. G. Kevrekidis, L. Lu, P. Perdikaris, S. Wang, and L. Yang, *Nature Reviews Physics* **3**, 422 (2021).
- [35] G. Carleo, I. Cirac, K. Cranmer, L. Daudet, M. Schuld, N. Tishby, L. Vogt-Maranto, and L. Zdeborová, *Reviews of Modern Physics* **91**, 045002 (2019).
- [36] T. D. Keidar and S. Reuveni, arXiv preprint arXiv:2410.16129 (2024).
- [37] S. Redner, *A Guide to First-Passage Processes* (Cambridge University Press, 2001).
- [38] R. Metzler, S. Redner, and G. Oshanin, *First-passage phenomena and their applications*, Vol. 35 (World Scientific, 2014).
- [39] A. J. Bray, Satya N. Majumdar, and G. Schehr, *Advances in Physics* **62**, 225 (2013).
- [40] S. Reuveni, *Physical review letters* **116**, 170601 (2016).
- [41] A. Pal and S. Reuveni, *Physical review letters* **118**, 030603 (2017).
- [42] M. R. Evans, S. N. Majumdar, and G. Schehr, *Journal of Physics A: Mathematical and Theoretical* **53**, 193001 (2020).
- [43] O. Blumer, S. Reuveni, and B. Hirshberg, *The journal of physical chemistry letters* **13**, 11230 (2022).
- [44] O. Blumer, S. Reuveni, and B. Hirshberg, *Nature Communications* **15**, 240 (2024).
- [45] I. Eliazar and S. Reuveni, *Journal of Physics A: Mathematical and Theoretical* **53**, 405004 (2020).
- [46] A. Nitzan, *Chemical dynamics in condensed phases: relaxation, transfer, and reactions in condensed molecular systems* (Oxford university press, 2024).
- [47] W. Ji, W. Qiu, Z. Shi, S. Pan, and S. Deng, *The Journal of Physical Chemistry A* **125**, 8098 (2021).
- [48] H. A. Kramers, *physica* **7**, 284 (1940).
- [49] P. Hanggi, *Journal of Statistical Physics* **42**, 105 (1986).
- [50] P. Hänggi, P. Talkner, and M. Borkovec, *Reviews of modern physics* **62**, 251 (1990).
- [51] A. Krizhevsky, G. Hinton, *et al.*, *Learning multiple layers of features from tiny images*, Master’s thesis, Toronto, ON, Canada (2009).
- [52] K. He, X. Zhang, S. Ren, and J. Sun, in *Proceedings of the IEEE conference on computer vision and pattern recognition* (2016) pp. 770–778.
- [53] A. Barducci, M. Bonomi, and M. Parrinello, *Wiley Interdisciplinary Reviews: Computational Molecular Science* **1**, 826 (2011).
- [54] O. Valsson and M. Parrinello, *Physical review letters* **113**, 090601 (2014).
- [55] G. Bussi and A. Laio, *Nature Reviews Physics* **2**, 200 (2020).
- [56] F. J. Massey Jr, *Journal of the American statistical Association* **46**, 68 (1951).
- [57] P. Tiwary, J. Mondal, J. A. Morrone, and B. Berne, *Proceedings of the National Academy of Sciences* **112**, 12015 (2015).
- [58] O. Blumer, S. Reuveni, and B. Hirshberg, *Journal of Chemical Theory and Computation* **20**, 3484 (2024).
- [59] G. Leclerc, A. Ilyas, L. Engstrom, S. M. Park, H. Salman, and A. Mądry, in *Proceedings of the IEEE/CVF Conference on Computer Vision and Pattern Recognition* (2023) pp. 12011–12020.